TAPPING THE POTENTIAL OF ADAPTABLE CONTROL AND ESTIMATION METHODS FOR SPACECRAFT AOCS

Ramin Geshnizjani[(1)], Maurice Martin[(1)], Răzvan Luzi[(1)], Stefan Winkler[(1)], Iñigo Fernandez Imaña[(2)], Xavier Manuel Juanpere[(2)], Felix Biertümpfel[(3)], Harald Pfifer[(3)]

[(1)]*Airbus Defence and Space GmbH, Claude-Dornier-Str., 88090 Immenstaad, Germany, ⟨firstname.lastname⟩@airbus.com*
[(2)]*Airbus Defence and Space SAS, 31 Rue de Cosmonautes, 31402 Toulouse cedex 4, France, ⟨firstname.lastname⟩@airbus.com*
[(3)]*Chair of Flight Mechanics and Control, Technische Universität Dresden, 01062 Dresden, Germany, ⟨firstname.lastname⟩@tu-dresden.de*

ABSTRACT

With their theoretical basis now well understood, parameter-varying and adaptable control and estimation methods have been successfully applied to aircraft and launcher control problems. For spacecraft, the effect of time-varying parameters is less overt; nevertheless, explicitly considering parameter variations in the controller/estimator design process can be beneficial in some cases. This paper provides an overview of several parameter-varying satellite and spacecraft attitude control and estimation problems. The respective dynamics are briefly described and then reformulated in line with a (linear) parameter-varying framework.

1 INTRODUCTION

In the last decades, linear parameter-varying (LPV) and adaptable control methods have found their way into the aerospace domain. Their theoretical basis is now well understood and practical design tools are now readily available.
Examples of successful application of LPV methods include aircraft wing flutter control [30] and missile autopilots [7]; furthermore, LPV control designs exist for re-entry vehicles [18] and launchers [34]. Especially the latter can be considered a more than suitable application due to the small time constants and wide range of dynamical properties.
For satellites and spacecraft, on the other hand, the challenges posed by parameter variations are less overt. A major reason lies in the comparatively long time constants of the spacecraft dynamics and the environmental conditions.
Nevertheless, accounting for parameter variations in the controller design process can have benefits, some of which lie beyond typical closed-loop performance metrics. Motivated by the on-going ESA-funded study *Adaptable Attitude Control and Estimation with Guaranteed Robust Performance* (ACE), this paper discusses several challenges and opportunities of current practical interest that are connected with time-varying parameters.
The remainder of this paper is structured as follows: section 2 provides a brief recapitulation of LPV and adaptable control methods with particular focus on the aerospace domain. Sections 3 through 6 discuss some exemplary parameter-varying control and estimation problems relevant for spacecraft guidance, navigation and control (GNC). Finally, some conclusions are drawn in section 7.

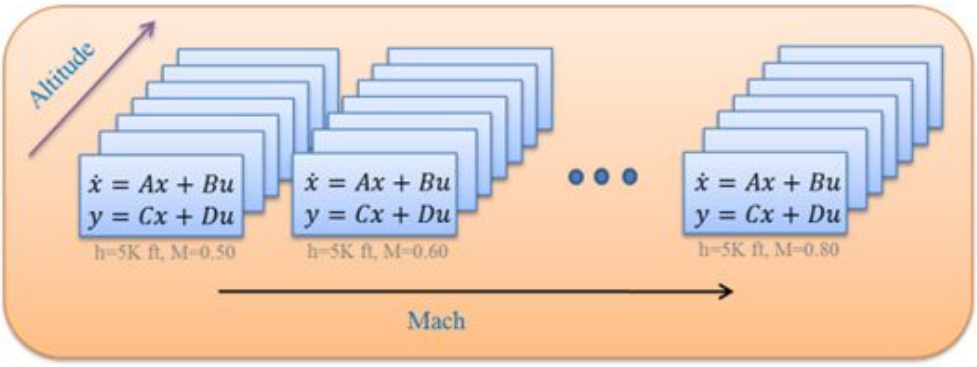

Figure 1: Concept of a Gridded LPV Model

2 PARAMETER-VARYING CONTROL AND ESTIMATION FOR AEROSPACE GNC SYSTEMS

2.1 Theoretical Background

LPV systems are a versatile mathematical modeling framework that is capable of representing the dynamic behavior of various complex engineering systems such as aircraft, wind turbines, and mechatronic systems, see e.g. [11] or [9] for an overview. LPV systems are dynamic systems whose state space representation involves continuous matrix functions of a time-varying parameter vector $\boldsymbol{\rho}$ that is not known in advance but measurable at each time instant:

$$\begin{aligned} \dot{\boldsymbol{x}}(t) &= \boldsymbol{A}(\boldsymbol{\rho}(t))\,\boldsymbol{x}(t) + \boldsymbol{B}(\boldsymbol{\rho}(t))\,\boldsymbol{u}(t) \\ \boldsymbol{y}(t) &= \boldsymbol{C}(\boldsymbol{\rho}(t))\,\boldsymbol{x}(t) + \boldsymbol{D}(\boldsymbol{\rho}(t))\,\boldsymbol{u}(t) \end{aligned} \tag{1}$$

with an unknown but measurable continuous function $\boldsymbol{\rho}\colon \mathbb{R}_+ \mapsto \mathcal{P} \subset \mathbb{R}^{n_\rho}$, where $\mathcal{P}$ is a compact set of admissible parameter values, and known continuous functions $\boldsymbol{A}(\boldsymbol{\rho}), \boldsymbol{B}(\boldsymbol{\rho}), \boldsymbol{C}(\boldsymbol{\rho})$, and $\boldsymbol{D}(\boldsymbol{\rho})$. For a fixed parameter value, the LPV system becomes an LTI system.

As first proposed by [1], both exogenous and endogenous parameter variations can be modeled in the framework of LPV systems. Exogenous parameters variations do not dependent on the system state and $\boldsymbol{\rho}(t)$ is often called "scheduling signal", which is a priori unknown but measurable online. Endogenous parameter variations dependent also on the state of the system, i.e. $\boldsymbol{\rho}(t, \boldsymbol{x}(t))$ is a function of the system state. The latter are captured by the quasi-LPV (qLPV) paradigm. The name originates from the fact that qLPV systems describe are nonlinear systems, expressed in a quasi linear form.

The attractiveness of the LPV framework is based on the availability of a large body of theoretical results for analysis and synthesis [3], [2], [6], [5], [4], [12], [13], [15], [16], [17] as well as mature computational tools [26]. As a consequence, LPV control can be used to apply powerful control design techniques from robust control theory to a wide class of nonlinear systems and to systems that are naturally modelled with parameter-dependent time-varying dynamics.

Two main types of LPV systems can be distinguished. The first are so called gridded LPV systems, which use a set of local models to represent the LPV system. A graphical representation is given in Fig. 1. The other are LPV-linear fractional transformation (LFT) models [20], [21]. If the parameter dependence of the model is rational in $\boldsymbol{\rho}$, a linear fractional representation can be used. It represents the LPV system as the interconnection of a linear time-invariant (LTI) model and a time-varying parameter block as depicted in Fig. 2. Specifically, the model from Eq. 1 can be expressed as

$$\mathcal{F}_{\mathrm{U}}(\boldsymbol{M}, \boldsymbol{\Delta}(\boldsymbol{\rho})) = \boldsymbol{M}_{22} + \boldsymbol{M}_{21}\,\boldsymbol{\Delta}(\boldsymbol{\rho})\,\left(\boldsymbol{I} - \boldsymbol{M}_{11}\,\boldsymbol{\Delta}(\boldsymbol{\rho})\right)^{-1}\,\boldsymbol{M}_{12}$$

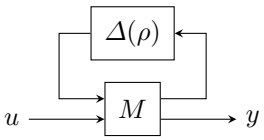

Figure 2: LPV System as LFT Model

where $\boldsymbol{M} = \begin{bmatrix} \boldsymbol{M}_{11} & \boldsymbol{M}_{12} \\ \boldsymbol{M}_{21} & \boldsymbol{M}_{22} \end{bmatrix}$ is parameter-independent and $\boldsymbol{\Delta}(\boldsymbol{\rho})$ contains the parameter dependence, similar to the representation of uncertainties in robust control.
Performance of LPV systems is usually specified in terms of the induced $\mathcal{L}_2$-norm from a performance input w to a performance output z. For the controller synthesis an optimization problem has to be solved over the set of all possible parameter trajectories $\mathcal{P}$:

$$\min_{\boldsymbol{K}_\rho, \boldsymbol{\rho} \in \mathcal{P}} \|\boldsymbol{P}_\rho * \boldsymbol{K}_\rho\|$$
$$\text{s. t. } \boldsymbol{K}_\rho \text{ stabilizes } \boldsymbol{P}_\rho$$

where the notation $*$ denotes the closed-loop interconnection and $\boldsymbol{P}_\rho$ denotes the LPV plant from Eq. 1.
Depending on how exactly the model depends on the scheduling parameter, several approaches exist that formulate the controller synthesis as a semidefinite program (SDP) based on two linear matrix inequalities (LMIs). A widely used approach is to solve the SDP over a gridded parameter space [6].

2.2 Application to Aerospace Systems

Numerous applications of LPV control to aerospace engineering problems can be found in literature. An elaborate example is the control of a turbofan engine in [14], where the power code of the engine is used as the scheduling parameter. Another prototypical application for LPV control is the rigid body motion of aircraft. The most common scheduling parameters are altitude and Mach number or the dynamic pressure. Examples for flight tested LPV controllers are [10] on board of the VAAC Harrier or [31] on board of a Cessna Citation. More recently, LPV control has been applied for flutter suppression of highly flexible wings [30]. LPV control has also been applied for missile autopilots [7]. In the scope of space applications, LPV control designs exist for ESA's Vega launcher [34] and re-entry vehicles [18]. However, these have not been flown yet.
Satellites and spacecraft have much slower dynamics than aircraft and launchers. For instance, the rotation of the solar arrays of an Earth observation satellite changes its mass properties at a rate of one revolution per orbit, which for low Earth orbits amounts to less than 0.1 deg/s. Furthermore, the rotation of such an appendage typically leads only to a small change of the spacecraft's moment of inertia (MoI). It is therefore not surprising that classical robust LTI control design methods are usually sufficient to fulfil stability and performance requirements of current satellite missions.
Nevertheless, accounting for parameter variations in the controller design process can have benefits, some of which lie beyond typical closed-loop performance metrics.
The current trend of commercialisation has introduced *product lines* into satellite development and production. Among a product line, individual satellites are mostly similar (or even identical), but may still differ from each other in terms of e.g. payload. As a result, many GNC relevant properties are constant along the product line, while some parameters such as the moment of inertia vary within certain bounds. A natural goal is therefore to aim for a single adaptable controller for the entire product line with suitable scheduling parameters to adapt the controller for each individual satellite. The main benefit is the increased efficiency of the controller design process itself, which becomes

Table 1: Comparison of Most Prominent LPV Toolboxes

Toolbox	Functionality	Limitations
LPVTools	model reduction, analysis, synthesis and simulation, LFT and gridded	No auto-balancing for control design, slow solvers for (standard) SDPs, Limited to up to 50 states, no imposable structure for the controller
LPVcore	modeling, identification and control of linear parameter-varying (LPV) systems, global setting	Early release, missing standard functionalities, standard SDP approach, no imposable structure for the controller
Robust Control Toolbox	Modelling, analysis and synthesis of uncertain systems, System order reduction, Structured robust control synthesis	No explicit LPV functionality

significant already in the extreme case of a "product line" of two satellites such as the MetOp-SG spacecraft.
This "product line approach" can even be transferred to the design process of a single spacecraft where relevant properties (especially mass and moment of inertia) are typically known only with large uncertainties in early design phases, but become more and more certain as the design matures. Compared with designing the controllers robust against the initial large uncertainty, the achievable performance could be increased by requiring robustness only against the final small uncertainties and treating the nominal parameter values in a parameter-varying framework.
On mission level, the ability to explicitly account for parameter variations enables additional operational modes. For example, some science spacecraft such as the envisaged Advanced Telescope for High-ENergy Astrophysics (ATHENA) mission contain several instruments that share the same optics, requiring large movable parts to align the correct detector to the line of sight [23]. Reorienting both the spacecraft and the movable parts simultaneously can save a significant amount of maneuvering time, thus increasing the scientific output.
Laser communication terminals require high pointing stability, but are subjected to structural vibrations with varying frequencies (e.g. reaction wheel induced microvibrations that depend on the wheel speeds). For this application, an adaptable disturbance estimation and cancellation scheme can allow using less performant (and thus, less expensive) hardware while still fulfilling all performance requirements.

2.3 Available Toolboxes

In addition to MATLAB's Robust Control Toolbox (RCT), mature tools for LPV analysis and synthesis exist. The two most prominent toolboxes, LPVtools [26] and LPVcore [32], will be discussed in the following. The discussion is summarized in Table 1. Both toolboxes are freely available and specifically developed for MATLAB, one of the most widespread programming and numeric computing platforms in engineering.
The functionality of both toolboxes is practically similar. They cover LPV modelling, model reduc-

tion, synthesis, and analysis. However, LPVTools focuses heavily on the gridded LPV approach. LPVcore distinguishes itself by also providing a so called global setting, i.e. time-varying scheduling trajectories. LPVTools is the more matured toolbox given LPVcore's initial release in 2021. The latter has still a limited functionality, which gets continuously extended.
Although quite evolved, LPV controller synthesis using the discussed tools summarized in Table 1 (but also in general) has three major issues:

1. The respective SDP scales badly with the number of state variables and scheduling parameters.
2. The resulting controller is a full-order dynamic controller without any exploitable structure.
3. The controller depends explicitly on the derivative of the scheduling parameters.

In summary, these result in the discussed scarce industrial application. With respect to the first issue, a general rule of thumb is to limit the number of scheduling parameters to three for gridded LPV systems. LFT LPV systems scale better with the number of parameters, if the dependency on them is simple, i.e. functions of low order.
Another notable tool, which however is not as easily accessible, is LPVMAD, which was developed in an ESA project with the same name [28]. An example for a toolbox specialised purely on identification is the LPV Input/Output Systems Identification Toolbox (LPVIOID) [27].
Another important toolbox is Matlab's build-in robust control toolbox [28]. Although not an explicit LPV toolbox, it provides a number of useful functionalities. These functionalities include, linear matrix inequality (LMI) tools, LFT modelling, structured singular value analysis (μ), worst-case gain analysis. Especially the LMI tools are an integral part in LPV analysis and synthesis as both problems are posed as LMIs. Moreover, the toolbox includes the powerful systune function [22] and the well-known structured $\mathcal{H}_\infty$ design [4]. Although it allows for automated gain scheduling, it is not an explicit LPV method. The Robust Control Toolbox is a well-established framework, which found its way into many applications of industrial complexity. This is particularly true for the $\mathcal{H}_\infty$ synthesis features.

3 MULTI-BODY SPACECRAFT WITH PRESCRIBED MOTIONS

3.1 Spacecraft with Rotating Appendages

MetOp-SG is an example of a spacecraft with rotating appendages. It can be modelled as a multi-body, which consists of a rigid main body, two scatterometers, and one solar array (S/A). To track the Sun, the S/A is rotating with respect to the main body. This influence is significant on the dynamics because the solar array is a large appendage and far away from the centre of mass of the main body. In particular it changes the MoI of the overall multi-body system and cantilever frequency of the flexible modes. By estimating the current rotation angle of the S/A, these changes of the dynamics are known. This information can be exploited by a controller to improve the overall system performance.
To show the change in the dynamics because of the S/A rotation, consider the dynamics of the multi-body model are briefly presented. The flexible dynamics of the S/A can be formulated as:

$$\ddot{\boldsymbol{\eta}} + \operatorname{diag}\{2\,\zeta_i\,\omega_i\}\,\dot{\boldsymbol{\eta}} + \operatorname{diag}\{\omega_i^2\}\,\boldsymbol{\eta} + \boldsymbol{L}_{\mathrm{rot}}\,\dot{\boldsymbol{\omega}}_{\mathrm{S/A}} + \boldsymbol{L}_{\mathrm{tr}}\,\ddot{\boldsymbol{r}}_{\mathrm{S/A}} = \mathbf{0} \tag{2}$$

where $\boldsymbol{\eta}$ are the modal coordinates, ζ_i and ω_i are the damping and natural frequency of the i-th flexible mode, $\boldsymbol{L}$ denote the rotational and translational modal participation factors, and $\dot{\boldsymbol{\omega}}_{\mathrm{S/A}}$ and $\ddot{\boldsymbol{r}}_{\mathrm{S/A}}$ are the angular and linear acceleration of the S/A. Eq. 2 is expressed in a coordinate frame fixed to the S/A.

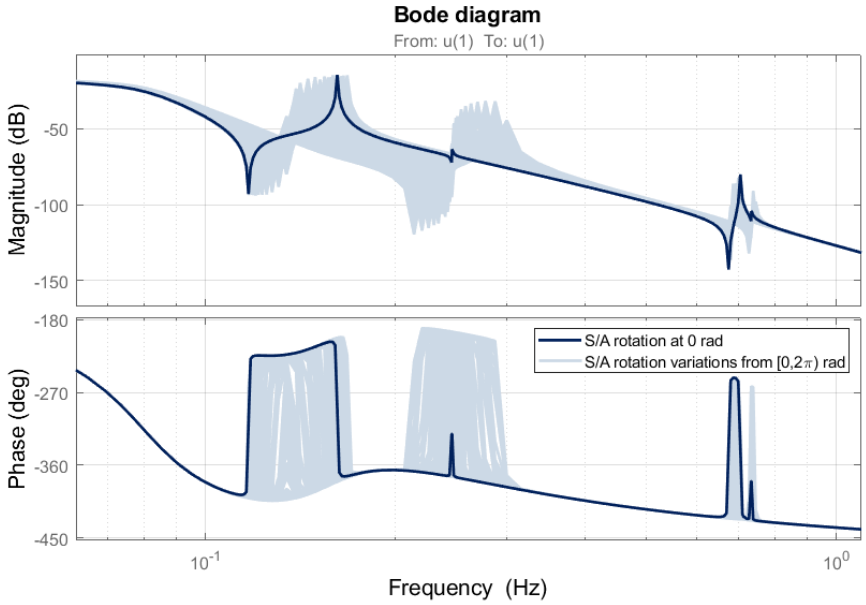

Figure 3: Exemplary Bode Plot of Multi-Body Model for MetOp-SG

These S/A flexibilities couple into the spacecraft's rotational dynamics via the participation factors:

$$\boldsymbol{J}\,\dot{\boldsymbol{\omega}} + \boldsymbol{\omega} \times \boldsymbol{J}\boldsymbol{\omega} + \dot{\boldsymbol{h}} + \boldsymbol{\omega} \times \boldsymbol{h} + \boldsymbol{L}_{\mathrm{rot}}^{\top}\,\ddot{\boldsymbol{\eta}} + m_{\mathrm{S/A}}\,\boldsymbol{r}_{CS} \times \ddot{\boldsymbol{r}} + \ddot{\boldsymbol{r}} \times \boldsymbol{L}_{\mathrm{tr}}^{\top}\boldsymbol{\eta} = \sum \boldsymbol{\tau} \tag{3}$$

In Eq. 3, all quantities must be expressed in the same core body-fixed frame. The rotation of the S/A changes the contributions of the participation factors $\boldsymbol{L}$ and thus the dynamical behavior. Specifically, the eigenfrequencies of the flexible modes change with the S/A rotation angle as shown in Fig. 3. In this example, the second flexible mode for the 0 rad does not participate much in the control axis whose Bode plot is shown in Fig. 3. However, by rotating the S/A the flexible mode becomes more visible in this control axis. This variation can significantly alter the stability and performance of the control loop. Therefore, this effect should be included in the controller design.
The classical approach is to design a LTI controller that is robust against all expected S/A rotation angles and thus covers the entire envelope of the flexible modes. This design is conservative because it treats the S/A rotation angles as an unknown uncertainty. Only one fixed controller is synthesized for all variants. Performance could be improved, however, by treating the S/A rotation as a varying parameter instead of an uncertainty, whose measurement is available in real time. This controller design is flexible to explicitly take into account the known dynamical changes and thus, expected to be more performant than the classical approach.
To design the flexible controller, the scheduling parameter is defined either in form of an LFT or in gridded form.
Without loss of generality the S/A rotation is assumed to be around the y-axis. The rotation of the S/A is described by the direction cosine matrix (DCM):

$$\boldsymbol{T}_{\mathrm{S/A}}(\theta) = \begin{bmatrix} \cos\theta & 0 & -\sin\theta \\ 0 & 1 & 0 \\ \sin\theta & 0 & \cos\theta \end{bmatrix} \tag{4}$$

The scheduling parameter in the DCM is the angle θ, which appears as arguments in trigonometric functions. However, the LFT formulation requires a polynomial expression with respect to the

scheduling parameter. Therefore, the terms $\sin\theta$ and $\cos\theta$ are rewritten as:

$$\sin\theta = \frac{4\,\rho\,(1-\rho^2)}{(1+\rho^2)^2}$$
$$\cos\theta = \frac{(1+\rho^2)^2 - 8\,\rho^2}{(1+\rho^2)^2}$$

with $\rho = \tan\theta/4$. The LFT formulation of Eq. 4 is therefore:

$$\boldsymbol{T}_{\mathrm{S/A}}(\rho) = \begin{bmatrix} \frac{(1+\rho^2)^2-8\,\rho^2}{(1+\rho^2)^2} & 0 & -\frac{(1+\rho^2)^2-8\,\rho^2}{(1+\rho^2)^2} \\ 0 & 1 & 0 \\ \frac{(1+\rho^2)^2-8\,\rho^2}{(1+\rho^2)^2} & 0 & \frac{(1+\rho^2)^2-8\,\rho^2}{(1+\rho^2)^2} \end{bmatrix}$$

A minimal representation of the DCM with eight repetitions of ρ can be found in [24].
An alternative to the LFT is the gridding approach. The S/A angle is gridded in sufficiently fine steps (e.g. $\rho_i = \{0°, 30°, \ldots, 330°\}$), which yields the gridded DCM:

$$\boldsymbol{T}_{\mathrm{S/A}}(\rho_i) = \begin{bmatrix} \cos\rho_i & 0 & -\sin\rho_i \\ 0 & 1 & 0 \\ \sin\rho_i & 0 & \cos\rho_i \end{bmatrix}$$

3.2 Multi-Body/Multi-Actuator Space Telescopes

Future space telescopes such as the envisaged ATHENA mission will contain multiple instruments that share the same optics, which for ATHENA is a mirror module. To align the line of sight to the observation target with the currently active detector, the mirror needs to be moved w.r.t. the spacecraft's main body by a dedicated mechanism such as a hexapod (see Fig. 4).

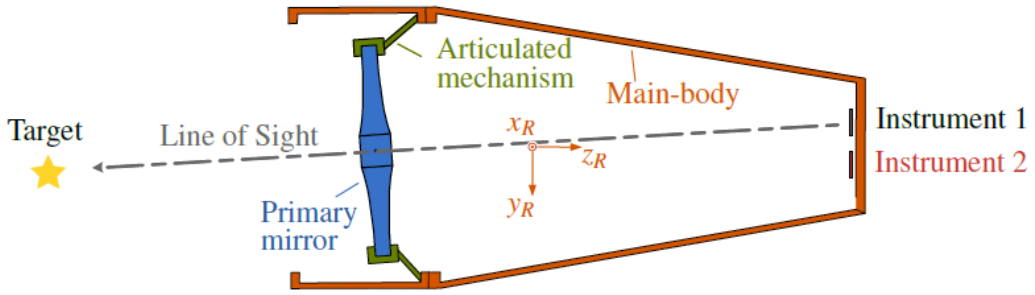

Figure 4: Space Telescope as Multi-Body/Multi-Actuator Spacecraft [35]

The rotational equations of motion (EoMs) of this multi-body system can be derived using e.g. d'Alambert's principle and have already been published in [29], [33]:

$$\begin{aligned} &{}_{\mathrm{B}}\boldsymbol{J}^{(B)}\ {}_{\mathrm{B}}\dot{\boldsymbol{\omega}}_{\mathrm{B/I}} + \left[{}_{\mathrm{B}}\boldsymbol{\omega}_{\mathrm{B/I}}\times\right]\ {}_{\mathrm{B}}\boldsymbol{J}^{(B)}\ {}_{\mathrm{B}}\boldsymbol{\omega}_{\mathrm{B/I}} \cdots \\ +\frac{m_{\mathrm{C}}\,m_{\mathrm{M}}}{m}&\left[{}_{\mathrm{B}}\boldsymbol{r}_{CM}\times\right]\ {}_{\mathrm{B}}\ddot{\boldsymbol{r}}_{CM} + \boldsymbol{T}_{\mathrm{BM}}\ {}_{\mathrm{M}}\boldsymbol{J}_{\mathrm{M}}^{(M)}\ {}_{\mathrm{M}}\dot{\boldsymbol{\omega}}_{\mathrm{M/B}} \cdots \\ &+\boldsymbol{T}_{\mathrm{BM}}\ {}_{\mathrm{M}}\boldsymbol{S}(\boldsymbol{J}_{\mathrm{M}}^{(M)}, \boldsymbol{\omega}_{\mathrm{M/B}})\,\boldsymbol{T}_{\mathrm{MB}}\ {}_{\mathrm{B}}\boldsymbol{\omega}_{\mathrm{B/I}} \cdots \\ &+\boldsymbol{T}_{\mathrm{BM}}\left[{}_{\mathrm{M}}\boldsymbol{\omega}_{\mathrm{M/B}}\times\right]\ {}_{\mathrm{M}}\boldsymbol{J}_{\mathrm{M}}^{(M)}\ {}_{\mathrm{M}}\boldsymbol{\omega}_{\mathrm{M/B}} \cdots \\ &+2\,\frac{m_{\mathrm{C}}\,m_{\mathrm{M}}}{m}\left[{}_{\mathrm{B}}\boldsymbol{r}_{CM}\times\right]\left[{}_{\mathrm{B}}\boldsymbol{\omega}_{\mathrm{B/I}}\times\right]\ {}_{\mathrm{B}}\dot{\boldsymbol{r}}_{CM} = \sum {}_{\mathrm{B}}\boldsymbol{\tau}_{\mathrm{ext}}^{(B)} \end{aligned} \tag{5}$$

In Eq. 5, a left subscript denotes the coordinate frame in which a quantity is expressed; specifically, the core body-fixed B frame centered at the *total* spacecraft's center of mass (CoM) B or the mirror-fixed M frame centered at the mirror's CoM M. The position of the mirror's CoM w.r.t. the core body's CoM is denoted by $\boldsymbol{r}_{CM}$ and $\boldsymbol{\omega}_{\mathrm{M/B}}$ denotes the mirror's angular rate w.r.t. the core body. The attitude of the mirror w.r.t. the (core) body is denoted by the DCM $\boldsymbol{T}_{\mathrm{MB}}$. The terms $\boldsymbol{J}^{(B)}$ and $\boldsymbol{J}_{\mathrm{M}}^{(M)}$ denote the MoI of the total spacecraft and the mirror, respectively, around their CoMs. Similarly, $\boldsymbol{\tau}_{\mathrm{ext}}^{(B)}$ denotes the sum of all external torques around B.
The first two terms of Eq. 5 are the rigid-body dynamics of the total spacecraft, whereas the third through seventh term are reaction torques acting on the spacecraft that are induced by the mirror's motion. For instance, the last term on the left hand side is a Coriolis effect.
The mirror's motion is performed by dedicated actuators, hence it can be considered a prescribed motion for the attitude control system. This allows a reformulation of the multi-body dynamics into a rigid-body spacecraft attitude control problem with parameter-varying mass properties. Specifically, the total MoI can be formulated as follows [33]:

$$\boldsymbol{J}^{(B)} = \boldsymbol{J}_{\mathrm{C}}^{(C)} + \boldsymbol{T}_{\mathrm{BM}}\,{}_{\mathrm{M}}\boldsymbol{J}_{\mathrm{M}}^{(M)}\,\boldsymbol{T}_{\mathrm{MB}} - \frac{m_{\mathrm{C}}\,m_{\mathrm{M}}}{m}\,\left[\boldsymbol{r}_{CM}\times\right]^2 \tag{6}$$

Denoting the mirror's nominal position and attitude by $\boldsymbol{r}_{CM_0}$ and $\boldsymbol{T}_{\mathrm{M_0B}}$, its true position and attitude can be formulated as $\boldsymbol{r}_{CM} = \boldsymbol{r}_{CM_0} + \Delta\boldsymbol{r}_{\mathrm{M}}$ and $\boldsymbol{T}_{\mathrm{MB}} = \boldsymbol{T}_{\mathrm{MM_0}}\,\boldsymbol{T}_{\mathrm{M_0B}} \approx (\boldsymbol{I} - [\boldsymbol{\varphi}\times])\,\boldsymbol{T}_{\mathrm{M_0B}}$, where we have used small-angle approximations for the mirror's angular motion w.r.t. its nominal attitude. Inserting these expressions into Eq. 6 yields

$$\boldsymbol{J}^{(B)} = \boldsymbol{J}_{0}^{(B)} + \Delta\boldsymbol{J}_{\mathrm{M}}(\boldsymbol{\rho}) \tag{7}$$

where $\boldsymbol{J}_{0}^{(B)}$ is the nominal MoI of the total spacecraft (i.e. with the mirror at its nominal pose) and $\Delta\boldsymbol{J}_{\mathrm{M}}(\boldsymbol{\rho})$ denotes the change of the MoI due to the mirror's motion. Note that the MoI change depends not only of mirror's pose change, but also on its nominal pose (the last term of Eq. 6 contains the product $[\boldsymbol{r}_{CM}\times]\;[\Delta\boldsymbol{r}_{\mathrm{M}}\times]$, which becomes a part of $\Delta\boldsymbol{J}_{\mathrm{M}}(\boldsymbol{\rho})$ in Eq. 7).
The scheduling parameter $\boldsymbol{\rho}$ consists of the mirror's pose change w.r.t. its nominal pose. In the most general case, it therefore represents six degrees of freedom. Eq. 7 is already in a form suitable for an LFT formulation. The LFT formulation of Eq. 7 can then be inverted using well-known methods [8]. As a result, the rigid-body dynamics subject to the prescribed mirror motion can be formulated as the LPV system

$$\boldsymbol{G}(s,\boldsymbol{\rho}) = \boldsymbol{J}^{-1}(\boldsymbol{\rho})\,\frac{1}{s^2}\,, \tag{8}$$

Eq. 8 can be extended by parametric uncertainties and flexible dynamics of solar arrays [e.g. 33].

4 VARIABLE DISTURBANCE ESTIMATION AND COMPENSATION FOR LASER COMMUNICATION TERMINALS

Laser communication terminals (LCTs) have the potential to provide unprecedented transmission rates to meet the needs of telecommunication satellites in the coming decades. LCTs are composed of several components, including a telescope that is responsible for routing the incoming and outgoing laser beams through optical lenses and reflectors, a coarse pointing mechanism (CPM) that is responsible for coarse pointing and large angular displacements, a fine pointing mechanism (FPM) that is responsible for fine pointing, an acquisition and tracking sensor (ATS) that is responsible for estimating the pointing errors, and Rx and Tx fibers that are used for communication to receive and send laser beams with data.

To establish the communication link between the satellite and the target, an acquisition sequence is used to ensure proper alignment of the line of sight (LoS). The acquisition sequence involves scanning using CPM to find the target beacon, centering of beacon using CPM, and establishment and maintenance of communication link using FPM for fine control and CPM for desaturation.
In terms of dynamics and modelization, the telescope and CPM can be considered as rigid bodies. The telescope provides the optical routing which can be modeled by gain transformations, and CPM is a flexible structure connecting the telescope to the satellite interface. As a first assumption, we can model the transfer between the input accelerations at the interface and the pointing error angle by a second-order system. The resonant mode is driven mainly by the CPM attitude. However, this transfer is supposed to be unknown. CPM transfer can be written in terms of fixed parameters and CPM frequency mode, ω_{n_C} :

$$H_{CPM}(s, \omega_{n_C}) = \frac{K_C \omega_{n_C}^2}{s^2 + 2\zeta_C \omega_{n_C} s + \omega_{n_C}^2} \tag{9}$$

CPM frequency is supposed to be dependent on CPM attitude, which changes over time. Nevertheless, regarding the control problem CPM modes can be considered to change quasi-statically, as its time of change is several orders of magnitude higher than the associated time to control bandwidth. Hence, the time dependency in CPM frequency has been removed.
The FPM can also be considered as a flexible structure that receives commands and produces an angular deflection of the incoming and outgoing beams. In a similar way, we can model the transfer between the commanded input signal and pointing error angle by a second-order system as a first assumption. However, this transfer is supposed to be known with some uncertainty in the mode frequency, $\omega_{n_F} = \omega_F + \Delta\omega_F$ and in the transfer gain $K_F = k_F + \Delta k_F$. However, in this case the FPM frequency is completely time independent:

$$H_{FPM}(s, \omega_{n_F}) = \frac{K_F \omega_{n_F}^2}{s^2 + 2\zeta_F \omega_{n_F} s + \omega_{n_F}^2} \tag{10}$$

In the sensor side, the ATS can be considered as well as a rigid body, and the transfer can be reduced to a gain H_{ATS}. During acquisition, an image is generated from the incoming photons and electrons. Then, image processing algorithms are used to compute the spot position and use this measurement for feedback control. There are several sources of errors during the whole detection process that might add measurement noise, n_{ATS}
The communication link is fragile, so high pointing stability is required to maintain data exchange. The main disturbances impacting the LCT pointing performance come from the platform (e.g., thermoelastics, solar array's rotation, Station-Keeping transients, star tracker noise, micro-vibrations), although there are also additional contributors introduced by the terminal itself (e.g., measurement errors, realization errors).
All platform disturbances are introduced at the interface level and consequently filtered/amplified by CPM behavior depending on the disturbance associated frequency. Micro-vibrations with similar frequencies to the CPM range are amplified and produce an important impact on Rx and Tx beams. Therefore, this is the main contributor to pointing accuracy.
There are several sources of micro-vibrations, but the main contributor is associated with the reaction wheels' angular rates used to control the spacecraft attitude. The disturbance generated from each RW can be modeled by a sinusoidal signal of a single variable frequency and amplitude, each of them varying with the angular rate of the RW. The magnitude of the disturbance is given by a specified envelope.
In the case of a satellite with 4 RWs, the micro-vibration disturbance coming from the RW could be modeled as 4 sinusoidal signals, $w_{mv,i}(t)$. By design, the angular rates of 2 of them can be kept out

of critical frequencies. However, the other 2 signals might coincide in the range of CPM frequency mode at the same time. Hence, the complete micro-vibration signal can be written as:

$$w_{mv}(t) = \sum_{i=1}^{2} A_{mv,i}(t) \sin\left(\omega_{mv,i}(t)\, t\right) \tag{11}$$

Where the initial phase of the disturbance has been set to zero without loss of generality.
The typical evolution of RW frequency during a complete orbit can be approached by two linear phases: one at a high-frequency rate and another one with a low-frequency rate. The angle rate of RWs close to CPM frequency modes are not equal, so crossings could happen during operation.
The main challenge arises when the frequency of micro-vibrations disturbance coincides with CPM frequency since it amplifies and could generate an important pointing error breaking the communication link.
To ensure a satisfactory rejection of the CPM-filtered disturbance, the controller H_{ctrl} should be designed to maximize its gain in the range of possible CPM resonance frequencies. In this case, the transfer between the micro-vibration signal and the pointing error can be written as:

$$S_{w\to\theta} = \frac{H_{CPM}}{1 + H_{FPM} H_{ctrl} H_{ATS}} \tag{12}$$

Since the controller must be robust to all the possible configurations of CPM modes, the classic approach would be to synthesize a high bandwidth controller to cover the micro-vibrations and respect the traditional stability criteria. Nevertheless, an adaptable estimator and controller could be used to improve tracking performances and potentially decreasing hardware requirements, thus enabling cost reduction.

5 PARAMETER-VARYING GYRO-STELLAR ESTIMATION

5.1 GSE with Moving Star Tracker

For multi-body/multi-actuator spacecraft architectures, the sensors need not necessarily be mounted on the same (sub-)body. Consider the case where the gyroscope is mounted on the core body, while the star trackers (STRs) are mounted on a movable minor body.
A typical gyro-stellar estimator (GSE) is a version of an extended Kalman filter (EKF) that updates the attitude estimation *error state* [25, Ch. 6.2]. The Kalman gain at time step t_k is computed as

$$\boldsymbol{K}_k = \boldsymbol{P}_k^- \boldsymbol{H}_k^\top \left(\boldsymbol{H}_k \boldsymbol{P}_k^- \boldsymbol{H}_k^\top + \boldsymbol{R}_k\right)^{-1}, \tag{13}$$

where $\boldsymbol{P}_k^-$ is the *a priori* estimation error covariance, $\boldsymbol{H}_k$ is the measurement matrix, and $\boldsymbol{R}_k$ is the STR noise covariance matrix. For many spacecraft, both the measurement matrix $\boldsymbol{H}$ and the STR noise covariance $\boldsymbol{R}$ are constant. As a result, the Kalman gain will converge to a constant value. To reduce the computational load, the Kalman gain can even be preset to the (expected) optimal value, i.e. the GSE becomes essentially a constant-gain EKF.
In our case, however, the STR's attitude w.r.t. the main body can change, hence $\boldsymbol{R}$ (which is expressed in the main body frame) is not constant anymore:

$$\boldsymbol{R}_k = \boldsymbol{T}_{\mathrm{BU},k}\, {}_{\mathrm{U}}\boldsymbol{R}\, \boldsymbol{T}_{\mathrm{BU},k}^\top = \boldsymbol{T}_{\mathrm{BU}_0}\, \Delta\boldsymbol{T}_k^\top\, {}_{\mathrm{U}}\boldsymbol{R}\, \Delta\boldsymbol{T}_k\, \boldsymbol{T}_{\mathrm{BU}_0}^\top \tag{14}$$

In Eq. 14, ${}_{\mathrm{U}}\boldsymbol{R}$ is the STR noise covariance matrix expressed in its unit frame, which is constant. The varying parameter is the attitude of the STR w.r.t. the main body $\boldsymbol{T}_{\mathrm{BU},k}^\top$, which can be split up into the constant nominal attitude $\boldsymbol{T}_{\mathrm{BU}_0}$ and the deviation $\Delta\boldsymbol{T}_k$ from the nominal attitude.

From Kalman filter theory, Eq. 13 is the gain that minimizes the trace of the *a posteriori* estimation error covariance $\boldsymbol{P}_k^+$ [19, Ch. 3.3]. In the derivation, the matrices $\boldsymbol{P}_k^-$, $\boldsymbol{H}_k$, and $\boldsymbol{R}_k$ are allowed to be time-varying. Therefore, updating Eq. 14 at each time step with the current STR alignment and inserting into Eq. 13 yields the optimal instantaneous Kalman gain.
From a practical point of view, the improvement of attitude estimation performance (including a reduction of the settling time of the filter) has to be traded against the additional computational load. As on-board computers become more powerful, we expect the latter factor to become less important over time.

5.2 GSE for Agile Spacecraft

The continuous-time process model of a three-axis GSE is [25, p. 245]:

$$\begin{pmatrix} \delta\dot{\boldsymbol{\alpha}} \\ \delta\dot{\boldsymbol{\beta}} \end{pmatrix} = \begin{bmatrix} -[\hat{\boldsymbol{\omega}}\times] & \boldsymbol{0} \\ \boldsymbol{0} & \boldsymbol{0} \end{bmatrix} \begin{pmatrix} \delta\boldsymbol{\alpha} \\ \delta\boldsymbol{\beta} \end{pmatrix} + \begin{bmatrix} -\boldsymbol{I} & \boldsymbol{0} \\ \boldsymbol{0} & \boldsymbol{I} \end{bmatrix} \begin{pmatrix} \boldsymbol{\nu}_{\mathrm{arw}} \\ \boldsymbol{\nu}_{\mathrm{rrw}} \end{pmatrix} \tag{15}$$

The estimation states are the small angle representation $\delta\boldsymbol{\alpha}$ of attitude estimation error and the gyro bias estimation error $\delta\boldsymbol{\beta}$. The process noise inputs are the angular random walk $\boldsymbol{\nu}_{\mathrm{arw}}$ and the rate random walk $\boldsymbol{\nu}_{\mathrm{rrw}}$.
The state matrix of the filter contains the current estimate of the angular rate $\hat{\boldsymbol{\omega}}$. For Nadir- or inertial pointing spacecraft, the true angular rate (and for a functioning GSE, also its estimate) is approximately constant. During rotation maneuvers, however, Eq. 15 describes a LPV system where the angular rate estimate is the time-varying parameter (it is not part of the state, but it available in real-time from the filter's last propagation or update).

6 PARAMETER VARIATIONS DURING AOCS DESIGN

The uncertainty of the mass properties changes during the design of the spacecraft throughout the project phases. Initially, the MoI is not well known and a typical design uncertainty of 20 % is assumed. Towards the end of the project, the design of the spacecraft is fixed, so that the remaining uncertainty can reduce to around 3 %.
A simple gridded LPV model for the MoI change is given by the scaling of the MoI matrix as a whole:

$$\boldsymbol{J}(\rho_i) = \rho_i\, \boldsymbol{J} \qquad \rho_i \in [\rho_{\min}, \rho_{\max}]$$

Alternatively, an LFT model can be formulated as:

$$\mathcal{F}_{\mathrm{U}}(\boldsymbol{M}, \boldsymbol{\Delta}) = \mathcal{F}_{\mathrm{U}} \left(\begin{bmatrix} \boldsymbol{0} & \sqrt{r}\,\boldsymbol{J}^{1/2} \\ \sqrt{r}\,\boldsymbol{J}^{1/2} & \boldsymbol{J}^{1/2} \end{bmatrix} ,\ \delta_J\, \boldsymbol{I} \right)$$

where r is the relative uncertainty of $\boldsymbol{J}$ (e.g. 20 %). The matrix square root exists because the inertia matrix is symmetric and positive definite.

7 CONCLUSIONS

Despite comparatively slow dynamics, parameter-varying effects are worth considering for some spacecraft GNC problems. As illustrated by the examples discussed in this paper, the parameter variations sometimes do not affect the dynamics directly, but have an impact on the design process itself. Also, explicitly considering parameter variations may not improve classical control performance and robustness metrics, but can improve e.g. *mission* performance or design cost.
Future work will focus on the definition of suitable indicators whether robust LTI methods are sufficient or whether parameter-varying techniques should be used to meet the requirements.

ACKNOWLEDGMENTS

This work was supported by the European Space Agency (Contract No. 4000137027/21/NL/MGu) in the context of the Open Invitations To Tender (ITT) "Adaptable Attitude Control and Estimation with Guaranteed Robust Performance" (AO/1-11017/21/NL/MGu).

REFERENCES

[1] J. S. Shamma, "Analysis and design of gain scheduled control systems," Ph.D. dissertation, 1988.

[2] G. Becker and A. Packard, "Robust performance of linear parametrically varying systems using parametrically-dependent linear feedback," *Systems & Control Letters*, vol. 23, no. 3, pp. 205–215, Sep. 1994. DOI: 10.1016/0167-6911(94)90006-x.

[3] A. Packard, "Gain scheduling via linear fractional transformations," *Systems & Control Letters*, vol. 22, no. 2, pp. 79–92, Feb. 1994. DOI: 10.1016/0167-6911(94)90102-3.

[4] P. Apkarian, P. Gahinet, and G. Becker, "Self-scheduled H∞ control of linear parameter-varying systems: a design example," *Automatica*, vol. 31, no. 9, pp. 1251–1261, Sep. 1995. DOI: 10.1016/0005-1098(95)00038-x.

[5] G. D. Wood *et al.*, "Control of parameter-dependent mechanical systems," Ph.D. dissertation, Citeseer, 1995.

[6] F. Wu, *Control of linear parameter varying systems*. University of California, Berkeley, 1995.

[7] F. Wu, A. Packard, and G. Balas, "LPV control design for pitch-axis missile autopilots," in *Proceedings of 1995 34th IEEE Conference on Decision and Control*, IEEE, 1995. DOI: 10.1109/cdc.1995.478672.

[8] G. J. Balas, J. C. Doyle, K. Glover, A. Packard, and R. Smith, *μ-Analysis and Synthesis Toolbox*, The MathWorks Inc., 1998.

[9] D. J. Leith and W. E. Leithead, "Survey of gain-scheduling analysis and design," *International Journal of Control*, vol. 73, no. 11, pp. 1001–1025, Jan. 2000. DOI: 10.1080/002071700411304.

[10] G. Papageorgiou, K. Glover, G. D'Mello, and Y. Patel, "Taking robust LPV control into flight on the VAAC harrier," in *Proceedings of the 39th IEEE Conference on Decision and Control (Cat. No.00CH37187)*, IEEE, 2000. DOI: 10.1109/cdc.2001.914633.

[11] W. J. Rugh and J. S. Shamma, "Research on gain scheduling," *Automatica*, vol. 36, no. 10, pp. 1401–1425, Oct. 2000. DOI: 10.1016/s0005-1098(00)00058-3.

[12] W. Tan, A. K. Packard, and G. J. Balas, "Quasi-LPV modeling and LPV control of a generic missile," in *Proceedings of the 2000 American Control Conference.*, IEEE, 2000. DOI: 10.1109/acc.2000.879259.

[13] C. W. Scherer, "LPV control and full block multipliers," *Automatica*, vol. 37, no. 3, pp. 361–375, Mar. 2001. DOI: 10.1016/s0005-1098(00)00176-x.

[14] G. J. Balas, "Linear, parameter-varying control and its application to a turbofan engine," *International Journal of Robust and Nonlinear Control*, vol. 12, no. 9, pp. 763–796, 2002. DOI: 10.1002/rnc.704.

[15] J. M. Rieber and F. Allgöwer, "An approach to gain-scheduled ℓ_1-optimal control of linear parameter-varying systems," in *42nd IEEE International Conference on Decision and Control (IEEE Cat. No.03CH37475)*, IEEE, 2003. DOI: 10.1109/cdc.2003.1272242.

[16] J. M. Rieber, C. W. Scherer, and F. Allgöwer, "Robust ℓ_1 Performance Analysis in face of Parametric Uncertainties," in *Proceedings of the 45th IEEE Conference on Decision and Control*, IEEE, Dec. 2006. DOI: 10.1109/cdc.2006.377748.

[17] J. M. Rieber, C. W. Scherer, and F. Allgöwer, "Robust ℓ_1 performance analysis for linear systems with parametric uncertainties," *International Journal of Control*, vol. 81, no. 5, pp. 851–864, May 2008. DOI: 10.1080/00207170701730451.

[18] A. Marcos and S. Bennani, "A linear parameter varying controller for a re-entry vehicle benchmark," in *Advances in Aerospace Guidance, Navigation and Control*, Springer Berlin Heidelberg, 2011, pp. 15–27. DOI: 10.1007/978-3-642-19817-5_2.

[19] J. L. Crassidis and J. L. Junkins, *Optimal Estimation of Dynamic Systems*. Taylor & Francis Inc, 2012, 749 pp., ISBN: 1439839859.

[20] S. Hecker and H. Pfifer, "Generation of LPV models and LFRs for a nonlinear aircraft model," in *Lecture Notes in Control and Information Sciences*, Springer Berlin Heidelberg, 2012, pp. 39–57. DOI: 10.1007/978-3-642-22627-4_3.

[21] J. Mohammadpour and C. W. Scherer, *Control of linear parameter varying systems with applications*. Springer Science & Business Media, 2012.

[22] P. Apkarian, P. Gahinet, and C. Buhr, "Multi-model, multi-objective tuning of fixed-structure controllers," in *2014 European Control Conference (ECC)*, IEEE, Jun. 2014. DOI: 10.1109/ecc.2014.6862200.

[23] European Space Agency, "CDF Study Report: ATHENA," European Space Agency, Tech. Rep. CDF-150(A), Nov. 2014.

[24] N. Guy, D. Alazard, C. Cumer, and C. Charbonnel, "Dynamic modeling and analysis of spacecraft with variable tilt of flexible appendages," *Journal of Dynamic Systems, Measurement, and Control*, vol. 136, no. 2, Jan. 2014. DOI: 10.1115/1.4025998.

[25] F. L. Markley and J. L. Crassidis, *Fundamentals of Spacecraft Attitude Determination and Control*. Springer New York, 2014. DOI: 10.1007/978-1-4939-0802-8.

[26] A. Hjartarson, P. Seiler, and A. Packard, "LPVTools: A toolbox for modeling, analysis, and synthesis of parameter varying control systems," *IFAC-PapersOnLine*, vol. 48, no. 26, pp. 139–145, 2015. DOI: 10.1016/j.ifacol.2015.11.127.

[27] M. Rabeei, H. S. Abbas, and M. M. Hassan, "Lpvioid: An lpv input/output systems identification toolbox using matlab," *URL sites. google. com/site/mustafarabeei*, 2015.

[28] *MATLAB version 9.3.0.713579 (R2017b)*, The Mathworks, Inc., Natick, Massachusetts, 2017.

[29] T. Ott, S. Görries, A. Schleicher, and S. Winkler, "AOCS design for the ATHENA X-ray telescope: Challenges and Solutions," in *10th International ESA Conference on Guidance, Navigation & Control*, 2017.

[30] J. Theis and H. Pfifer, "Observer-based synthesis of linear parameter-varying mixed sensitivity controllers," *International Journal of Robust and Nonlinear Control*, vol. 30, no. 13, pp. 5021–5039, Jul. 2020. DOI: 10.1002/rnc.5038.

[31] C. Weiser, D. Ossmann, and G. Looye, "Design and flight test of a linear parameter varying flight controller," *CEAS Aeronautical Journal*, vol. 11, no. 4, pp. 955–969, Aug. 2020. DOI: 10.1007/s13272-020-00461-y.

[32] P. den Boef, P. B. Cox, and R. Tóth, "LPVcore: MATLAB toolbox for LPV modelling, identification and control," *IFAC-PapersOnLine*, vol. 54, no. 7, pp. 385–390, 2021. DOI: 10.1016/j.ifacol.2021.08.390.

[33] A. Ponche, A. Marcos, T. Ott, and A. Schleicher, "Investigation of multi-body/multi-actuator modeling techniques for applicability to future space observation missions," in *11th International ESA Conference on Guidance, Navigation & Control*, held virtually from ESTEC, 2021.

[34] D. Navarro-Tapia, A. Marcos, and S. Bennani, "The VEGA launcher atmospheric control problem: A case for linear parameter-varying synthesis," *Journal of the Franklin Institute*, vol. 359, no. 2, pp. 899–927, Jan. 2022. DOI: 10.1016/j.jfranklin.2021.07.057.

[35] A. Ponche, A. Marcos, T. Ott, R. Geshnizjani, and J. Löhr, "Advanced Guidance Approach for Multi-Body/Multi-Actuator Spacecraft Repointing under Attitude Constraints," in *9th European Conference for Aeronautics and Space Sciences (EUCASS)*, Jun. 2022. DOI: 10.13009/EUCASS2022-6149.